INTERNATIONAL JOURNAL FOR NUMERICAL METHODS IN FLUIDS
Int. J. Numer. Meth. Fluids 2004; **45**:581–604 (DOI: 10.1002/fld.708)

3D two phase flows numerical simulations by SL-VOF method

Benjamin Biausser[1,2], Stephan Guignard[3], Richard Marcer[1] and Philippe Fraunié[2,*,†]

[1]*Principia R&D S.A., Z.I. Bregaillon, 83507 La Seyne-sur-mer Cedex, France*
[2]*LSEET, UMR 6017 du CNRS, Université de Toulon et du Var, B.P. 132, 83957 La Garde Cedex, France*
[3]*IRPHE, Technopóle de Château-Gombert-49, rue Joliot Curie-B. 146-13384 Marseille Cedex 13, France*

SUMMARY

This paper describes the development of a semi-Lagrangian computational method for simulating complex 3D two phase flows. The Navier–Stokes equations are solved separately in both fluids using a robust pseudo-compressibility method able to deal with high density ratio. The interface tracking is achieved by the segment Lagrangian volume of fluid (SL-VOF) method. The 2D SL-VOF method using the concepts of VOF, piecewise linear interface calculation (PLIC) and Lagrangian advection of the interface is herein extended to 3D flows. Three different test cases of SL-VOF 3D are presented for validation and comparison either with 2D flows or with other numerical methods. A good agreement is observed in each case. Copyright © 2004 John Wiley & Sons, Ltd.

KEY WORDS: volume of fluid; Rayleigh–Taylor instability; interface tracking; Navier–Stokes

1. INTRODUCTION

The importance of free-surface flows or more generally two-phase flows in recent research and industrial applications has led to the elaboration of improved numerical techniques. The numerical simulation of two phase flows with sharp interfaces requires simultaneous solution of the Navier–Stokes equations in the two fluids together and tracking of the interface kinematics. Different kinds of interface tracking methods have been developed [1]. We made the choice to develop a VOF approach because of its ability to represent complex deformation of an interface including reconnection, on the contrary of other accurate classical methods such as Lagrangian–Eulerian methods (ALE) [2] or boundary integral elements methods (BIEM) [3].

*Correspondence to: P. Fraunié, LSEET, UMR 6017 du CNRS, Université de Toulon et du Var, B.P. 132, 83957 La Garde Cedex, France.
†E-mail: phillipe.fraunie@lseet.univ-tln.fr

Contract/grant sponsor: Principia R. and D.
Contract/grant sponsor: French National Programme

Published online 19 April 2004

Received 9 November 2002
Revised 27 October 2003

The volume of fluid (VOF) concept has been initially introduced by Hirt and Nichols [4] through the SOLAVOF algorithm. In the original method, the interface was characterized by the fraction of the grid cell occupied by the denser fluid and was represented by segments (or planes in 3D) imposed to be parallel to the grid faces. The standard VOF method is very easy to use and to extend to 3D computations but has a zero order accuracy.

For this reason, several authors have improved the primitive VOF concept. For instance, Li [5] proposed the well known piecewise linear interface calculation method (PLIC) which allows to represent the interface by segments (or planes in 3D) of any direction in each cell. The evolution of the interface is then performed with an advected flux algorithm which must verify a stability criterion of CFL type and so imposes a limitation of the time step of the simulation.

We present hereafter the 3D extension of the recently developed 2D SL-VOF method [6]. This new VOF approach uses the PLIC concept for the segmental (or planar) representation of the interface in combination with a Lagrangian time scheme driving the segments (or planes) advection. The SL-VOF method allows on one hand to increase the accuracy of the standard VOF algorithm and on the other hand to reduce the computational time by using a larger time step (CFL greater than one), whereas the classical PLIC method is unable to use CFLs greater than 0.5. After introducing the Navier–Stokes solver (CFD EOLE code developed by PRINCIPIA R&D), we give a brief review of the principles of SL-VOF method for 2D flows. Then we present the full 3D SL-VOF method and several academic examples of application: advection of a sphere in an horizontal velocity field, advection of a sphere in a distorting velocity field and the Rayleigh–Taylor instability.

2. THE NUMERICAL PROBLEM

2.1. Formulation

We consider two incompressible viscous fluids of different densities, separated by a moving interface. The effect of the surface tension is not taken into account for the academic applications considered here.

The unsteady 3D Navier–Stokes equations for the two phase flows are then written in the following semi-conservative form, in curvilinear formulation:

$$\frac{1}{J}\frac{\partial W}{\partial t}+\frac{\partial F}{\partial \xi}+\frac{\partial G}{\partial \eta}+\frac{\partial H}{\partial \chi}=\frac{R}{J} \tag{1}$$

where F, G and H are the flux terms and R the volumic forces source term:

$$F=\frac{1}{J}\begin{pmatrix} \rho\tilde{u} \\ \rho\tilde{u}u+\xi_x p-\vec{\nabla}(\xi)\cdot\vec{\tau}_x \\ \rho\tilde{u}v+\xi_y p-\vec{\nabla}(\xi)\cdot\vec{\tau}_y \\ \rho\tilde{u}w+\xi_z p-\vec{\nabla}(\xi)\cdot\vec{\tau}_z \end{pmatrix}, \quad G=\frac{1}{J}\begin{pmatrix} \rho\tilde{v} \\ \rho\tilde{v}u+\eta_x p-\vec{\nabla}(\eta)\cdot\vec{\tau}_x \\ \rho\tilde{v}v+\eta_y p-\vec{\nabla}(\eta)\cdot\vec{\tau}_y \\ \rho\tilde{v}w+\eta_z p-\vec{\nabla}(\eta)\cdot\vec{\tau}_z \end{pmatrix}$$

$$H = \frac{1}{J}\begin{pmatrix} \rho\tilde{w} \\ \rho\tilde{w}u + \chi_x p - \vec{\nabla}(\chi)\cdot\vec{\tau}_x \\ \rho\tilde{w}v + \chi_y p - \vec{\nabla}(\chi)\cdot\vec{\tau}_y \\ \rho\tilde{w}w + \chi_z p - \vec{\nabla}(\chi)\cdot\vec{\tau}_z \end{pmatrix}$$

$$W = \begin{pmatrix} 0 \\ \rho u \\ \rho v \\ \rho w \end{pmatrix}, \quad R = \begin{pmatrix} 0 \\ \rho f_x \\ \rho f_y \\ \rho f_z \end{pmatrix}$$

$$\tilde{u} = \xi_x u + \xi_y v + \xi_z w, \quad \tilde{v} = \eta_x u + \eta_y v + \eta_z w, \quad \tilde{w} = \chi_x u + \chi_y v + \chi_z w, \quad J = \frac{\partial(\xi,\eta,\chi)}{\partial(x,y,z)}$$

$$\vec{\tau}_x = \bar{\bar{\tau}}\cdot\vec{e}_x \quad \vec{\tau}_y = \bar{\bar{\tau}}\cdot\vec{e}_y \quad \vec{\tau}_z = \bar{\bar{\tau}}\cdot\vec{e}_z \quad \bar{\bar{\tau}} = \mu(\vec{\nabla}\vec{U} + \vec{\nabla}^t\vec{U})$$

with (ξ,η,χ) the curvilinear co-ordinates, J the Jacobian of the co-ordinates transformation, and $\mathbf{n} = (n_x, n_y, n_z)$ the normal vector to the interface. Additionally, (u,v,w) are the cartesian velocity components for each phase, $(\tilde{u},\tilde{v},\tilde{w})$ the contravariant velocity components, p the pressure, ρ the density, μ the molecular viscosity and $\bar{\bar{\tau}}$ the viscous stress tensor.

2.2. The pseudo-compressibility method

Time discretization is ensured using a fully implicit second order scheme. The solution of the non-linear system for the unknown values at step $n+1$ is based on the pseudo-compressibility method [7, 8] using the following concept: introducing a time-like variable τ, called pseudo-time, in Equation (1), one adds pseudo-unsteady terms which are derivatives of the unknowns at time level $n+1$ with respect to τ. Considering the semi-discretized equations at the time level $n+1$, the system is written:

$$\frac{1}{J}\frac{\partial\tilde{W}^{n+1}}{\partial\tau} + \frac{1}{J}\frac{3W^{n+1} - 4W^n + W^{n-1}}{2\Delta t} + \left(\frac{\partial F}{\partial\xi}\right)^{n+1} + \left(\frac{\partial G}{\partial\eta}\right)^{n+1} + \left(\frac{\partial H}{\partial\chi}\right)^{n+1} = \frac{R^{n+1}}{J} \tag{2}$$

with

$$\tilde{W} = \begin{pmatrix} \tilde{\rho} \\ \tilde{\rho}u \\ \tilde{\rho}v \\ \tilde{\rho}w \end{pmatrix}$$

The pseudo-density terms involve a new unknown $\tilde{\rho}$, called pseudo-density, which is imposed to remain positive. The pressure is calculated as a function of $\tilde{\rho}$ through an additional pseudo-state equation:

$$p^{n+1} = f(\tilde{\rho}^{n+1}) \tag{3}$$

The choice of the optimized pseudo-state equation is discussed in Viviand [7]. The system (2,3) is integrated step-by-step in pseudo-time variable, up to the convergence towards the numerical solution at time level $n+1$. This system is hyperbolic with respect to τ and is formally very close to Navier–Stokes equations for compressible flows, due to the presence of the same unknown $\tilde{\rho}$ in the continuity and momentum equations. The spatial discretization is ensured with an adaptation of the finite volume method on multi-block curvilinear deforming grids, using a centred scheme with artificial viscosity (this procedure allows to avoid uncoupling between odd and even cells) [9].

The scheme used in pseudo-time is the explicit five steps Runge–Kutta scheme, associated with an implicit residual smoothing technique. The maximum value of the pseudo-time step is fixed by the local CFL stability criterion. For each cell, one uses the maximum local value (local time step technique). The method is unconditionally stable with respect to the physical time step. Finally this method is especially robust to deal with two phase flows exhibiting a high liquid–gas density ratio.

3. SL-VOF: INTERFACE TRACKING METHOD

For each time step the interface and its evolution are obtained by an original method, called SL-VOF [6], based on both VOF and PLIC [5] concepts. In each cell, the interface is represented by a discrete function C, the value of which is the volumic fraction of the denser fluid (VOF concept).

The general SL-VOF algorithm contains three main parts, namely the interface modelling, the interface advection and the reconstruction of the new VOF field, deduced from the interface location after advection. This procedure can be summarized by the following scheme:

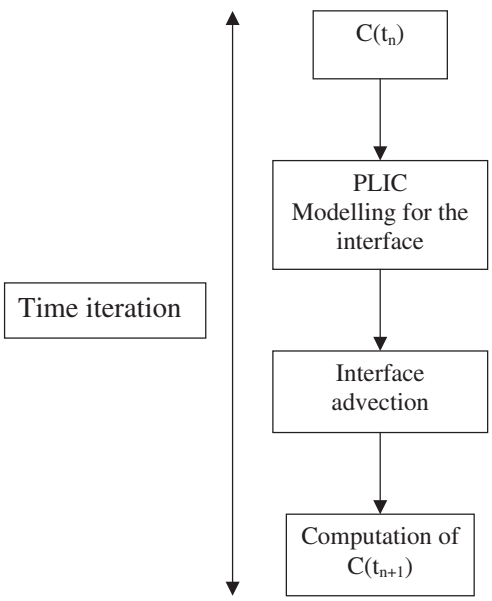

The used curvilinear formulation allows us to deal with a transformed mesh of unit cartesian cells (unit squares for the 2D method or unit cubes for the 3D method). In the next sections, only unit cells will be considered for the method description.

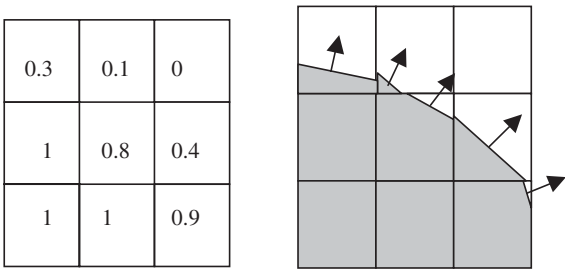

Figure 1. PLIC modelling of the interface: (a) Values of C in each cell and (b) PLIC model.

3.1. SL-VOF method for 2D flows

3.1.1. Interface modelling. In the original SOLAVOF [4] method, the interface was assumed to be parallel to the grid faces, so the accuracy of the method remained low. The first order PLIC method allows the interface to be represented by segments of any orientation. To define a unique segment in each cell, two parameters are necessary:

- the VOF value in the grid cell and
- the normal to the interface in the cell

The VOF field is kept from the last time step, so it is only necessary to define the normal direction to the segment. As shown in Figure 1, the normal **n** to the interface is defined as $-\vec{\nabla}C/\|\vec{\nabla}C\|$. From this definition, the normal is oriented from the denser to the less dense fluid. Thus, it is possible to represent the interface by a segment normal to **n** whose position is translated in order to satisfy the value of C in this cell. This representation does not ensure a continuous representation of the interface as a continuous linear interface would not satisfy the cells volume fraction. The co-ordinates of $-\vec{\nabla}C$ are computed using an eight point finite-differences discretization:

$$n_x = \frac{1}{8h_i}\left[2(C_{i+1,j} - C_{i-1,j}) + C_{i+1,j+1} - C_{i-1,j+1} + C_{i+1,j-1} - C_{i-1,j-1}\right]$$

$$n_y = \frac{1}{8h_j}\left[2(C_{i,j+1} - C_{i,j-1}) + C_{i+1,j+1} - C_{i+1,j-1} + C_{i-1,j+1} - C_{i-1,j-1}\right]$$

with (h_i, h_j) the local space discretization steps.

Once the normal direction is known, the segment has to be translated in the cell in order to respect the value of C. The segment is the line of equation: $n_x x + n_y y = \alpha$, where α is the parameter to be adjusted. Let us consider a unit cell whose origin is in $(0,0)$. By symmetry, it is always possible to consider that $0 < n_x \leqslant n_y$. The segments of normal directions (n_x, n_y) intercepting the points $(1,0)$ or $(0,1)$ generate 2 critical volumic fractions: $C_1 = n_x/2n_y$ and $C_2 = 1 - C_1$ (see Figure 2).

Then, there are three different possible expressions for α depending on the value of C:

- if $0 \leqslant C \leqslant C_1$ then $\alpha = \sqrt{2Cn_x n_y}$

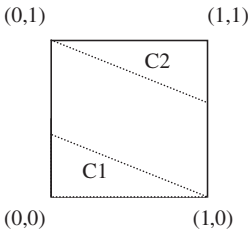

Figure 2. Critical volumic fractions.

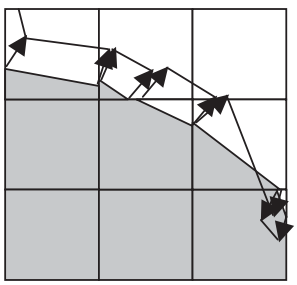

Figure 3. Advection of the segments (the arrows represent the velocity vectors).

- if $C_1 < C < C_2$ then $\alpha = (2Cn_y + n_x)/2$
- if $C_2 \leqslant C \leqslant 1$ then $\alpha = n_x + n_y - \sqrt{2(1-C)n_x n_y}$

Now, the equation of the segment is determined and it is possible to translate it correctly in the cell.

3.1.2. Interface advection. The displacement of the segments is computed in a Lagrangian way. The velocities at the ends of the segments are deduced from the general velocity field computed by the solver by a bilinear interpolation. The ends of the segments are then advected using a first-order Lagrangian scheme:

$$\mathbf{x}(t + \Delta t) = \mathbf{x}(t) + \Delta t \cdot \mathbf{u}$$

where $\mathbf{x}$ denotes the position of the ends of the segments, Δt the time step and $\mathbf{u}$ the velocity at the ends of the segments. The advection step is described in Figure 3.

3.1.3. Computation of C^{n+1}. As previously stated, due to the Lagrangian nature of SL-VOF method, there is no need to solve a conservation equation of the VOF function. So, one of the advantages of this new method in comparison to the former PLIC method and the original SOLAVOF algorithm, is to be able to use larger time steps. Considering the quantity $\mathrm{CFL}_{\mathrm{vof}}$ to be the maximum value of the ratio of the displacement of a fluid element at the interface during a time step to the maximum size of this cell, the earlier VOF methods were limited by the stability criterion $\mathrm{CFL}_{\mathrm{vof}} < 0.5$ [4, 5, 10]. The SL-VOF method has no theoretical constraint about the $\mathrm{CFL}_{\mathrm{vof}}$ criterion, which allows for a significant earn in computational time.

Moreover, recently an implicit procedure has been implemented: the interface is activated during the pseudo-time iterations (not only at the end of the pseudo-time iterations), which allows to increase the global CFL, and to reduce once more the computational time.

This step describes the computation of the new VOF field. In contrast to the original PLIC method [5] which uses a multi-step flux calculation to compute the value of C^{n+1}, SL-VOF deduces C^{n+1} from the new positions of the segments after advection unstead of solving the VOF transport equation. Numerical experiments have shown that even for complex interfaces, the volume conservation defect is not found critical enough (see Plate 3) to justify a fully VOF conservative procedure when the interface advection accuracy has been shown to be more important [6].

For this purpose, markers are uniformly dispatched on each segment. To each marker M_i is associated the normal vector $\mathbf{n}_i$ of the segment to which it belongs. Then, after advection, there are two possible kinds of cells:

- A type cells containing at least one marker and
- B type cells without any marker

Let us consider an A type cell (Figure 4). To the marker M_i corresponds a value C_i calculated according to the PLIC concept (cf. Figure 4(a)). As there are several portions of segments in the cell, it is necessary to determine if the cell is becoming full (reconnection of interfaces) or not. To determine this, a test is made on the value of the scalar product $pr_{ij} = \mathbf{n}_i \cdot \mathbf{n}_j$, where i and j describe the markers present in the cell. If all the pr_{ij} are positive then the new value of the VOF will be a mean value of the C_i's in the cell, to which is added or subtracted the areas of the additional polygons (Figure 4(a)).

If at least one pr_{ij} is negative, it means that a reconnection of interfaces could occur in the cell. Segments could cross each others so that the cell is becoming full of liquid. It is the case if the sum of the C_i's is more than 1, and C^{n+1} is then imposed to be 1 (Figure 4(b)). If the sum of the C_i's is less than one, C^{n+1} is computed in the same way as previously.

Let us now consider a B type cell (Figure 5). There are again two possibilities: either the cell did not contain any segment before the advection of the interface, and so the value of C is not modified, or the cell has lost the interface during the time step. In this case, one has to detect whether the cell becomes empty or full of the denser fluid, after advection. A test is made on the value of $pr = \mathbf{n} \cdot \mathbf{d}$ where $\mathbf{d}$ is the displacement of the centre of the segment during advection. The cell is fixed full if $pr > 0$ and empty if not (Figure 5).

3.2. SL-VOF method for 3D flows

The extension of SL-VOF for 3D flows is presented hereafter. The basic ideas remain the same, but the geometrical feature becomes more complex.

3.2.1. Interface modelling. In 3D configuration, the segments become portions of planes. An unique portion of a plane is defined by the normal direction and the VOF value in the cell.

The calculation of the normal interface at the centre of a cell (i, j, k) is carried out considering the two following steps:

- a finite-difference scheme is firstly used to compute the normal vectors at each corner of the cell (i, j, k). For instance, the normal vector at the corner defined by

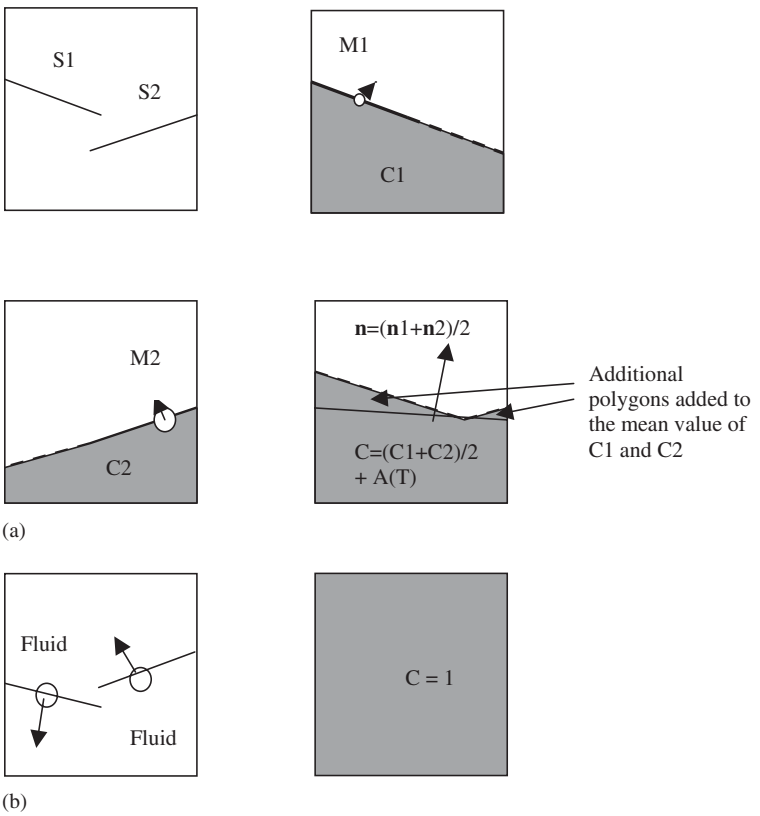

Figure 4. (a) Computation of C^{n+1} for an A type cell with two segments (no reconnection) S1 defines C1, S2 defines C2, C is the mean value of C1 and C2 plus the areas of the additional triangles; (b) Computation of C^{n+1} for an A type cell with two segments (reconnection).

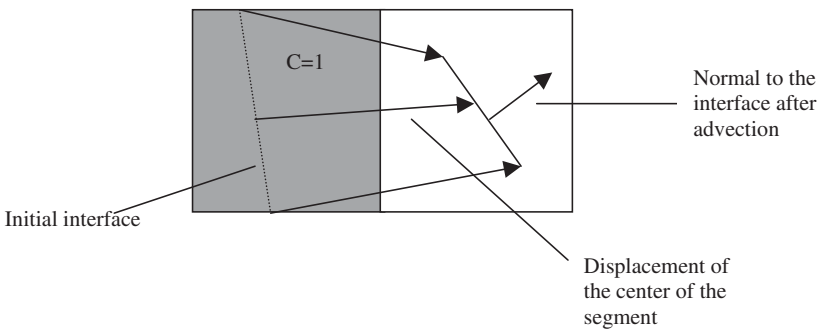

Figure 5. Computation of C^{n+1} for a B type cell case $d \cdot n > 0$.

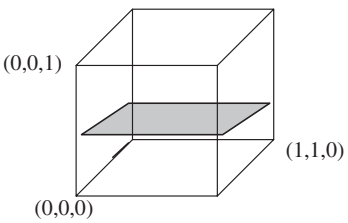

Figure 6. Cut cube.

$(i+1/2, j+1/2, k+1/2)$ will be:

$$\vec{n}_{i+\frac{1}{2},j+\frac{1}{2},k+\frac{1}{2}} = \frac{\vec{x}}{4h}\sum_{s,t=0}^{1}(F_{i+1,j+s,k+t} - F_{i,j+s,k+t}) + \frac{\vec{y}}{4h}\sum_{s,t=0}^{1}(F_{i+s,j+1,k+t} - F_{i+s,j,k+t}) + \frac{\vec{z}}{4h}\sum_{s,t=0}^{1}(F_{i+s,j+t,k+1} - F_{i+s,j+t,k})$$

In the same way, the normal vector is computed in the other corner of the cell (i,j,k).

- the normal vector $\mathbf{n}$ (n_x, n_y, n_z) at the centre of the cell (i,j,k) is then the mean value of the eight normal vectors at the corners.

Once the approximation of $\mathbf{n}$ is known, the plane has to be translated in the cell in order to satisfy the VOF function C in this cell. The equation of the plane is given by

$$n_x x + n_y y + n_z z = \alpha$$

where α is the unknown parameter. By symmetry, it is always possible to obtain that $0 < n_x < n_y < n_z$ $(=1)$. The volume of the cut cube generated by the plane increases from 0 to 1 when α increases from 0 to $n_x + n_y + n_z$. In 3D, it is necessary to distinguish eight cases [5] for the expression of the volume portion of the cube when cut by a polygon: six cases corresponding to a critical situation where the plane contains one corner of the cube and two additional particular cases (Figure 6) where the plane is first intercepting the corner $(1,1,0)$ and then the corner $(0,0,1)$ $(n_x + n_y < n_z)$, and the opposite situation $(n_x + n_y > n_z)$.

The six critical volumic fractions (i.e. the volumes corresponding to the cut cubes by the plane intercepting one corner) depend on the sign of $n_x + n_y - n_z$. This can be summarized by the following chart.

Critical volumic fractions depending on the normal orientation

	$C1$	$C2$	$C3$	$C4$	$C5$	$C6$
$n_x + n_y < n_z$	$\frac{1}{6}\frac{n_x^2}{n_y}$	$\frac{3n_x^2 - 3n_x n_y + n_y^2}{6n_x n_y}$	$\frac{1}{2}(n_x + n_y)$	1-$C3$	1-$C2$	1-$C1$
$n_x + n_y > n_z$	$\frac{1}{6}\frac{n_x^2}{n_y}$	$\frac{3n_x^2 - 3n_x n_y + n_y^2}{6n_x n_y}$	$\frac{1}{6n_x n_y}(1 - (1-n_x)^3 - (1-n_y)^3)$	1-$C3$	1-$C2$	1-$C1$

The classification of the geometrical shapes of the cut cubes allows to determine the shape of the polygon defined by the intersection of the plane and the cube. This polygon can have from

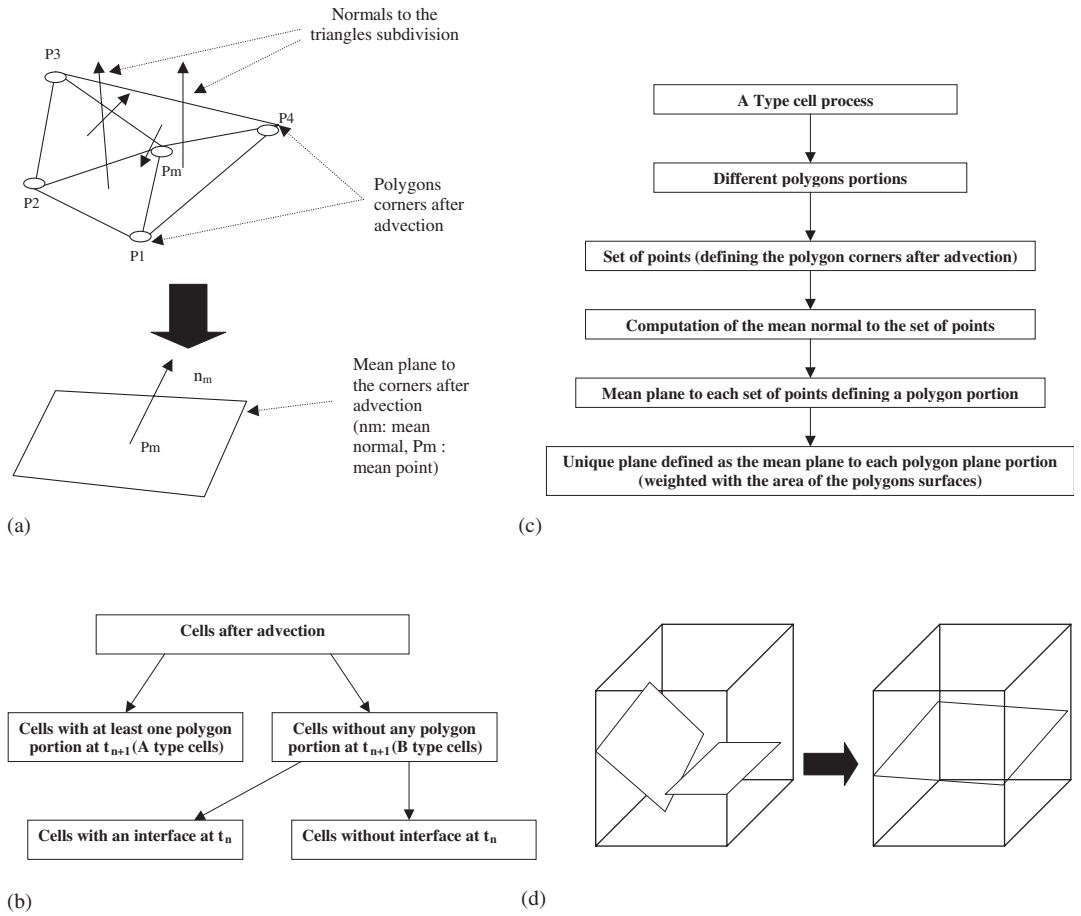

Figure 7. (a) Calculation of a mean plane to non-coplanar corners after advection; (b) General classification of the cells after advection; (c) General procedure for an A type cell; and (d) Definition of the mean plane for two polygons portions.

3 to 6 corners. Following the cases, it is possible to find the expression of α as a function of n and C (see Appendix A). An unique interface is then defined by this polygon.

3.2.2. Interface advection. The principle of the advection remains the same than for the 2D case. The velocities of the polygon corners are deduced from the velocity flow field, computed at the centre of the cells, using a bilinear interpolation. A first order in time Lagrangian scheme is then used to advect the corners. The main problem is that these points are not coplanar after advection, so it is necessary to define a mean plane deduced from this new set of points. This mean plane is defined in first order as the plane containing the centre of this set of points and whose normal is the mean of the normals to the triangles built with two consecutives points of the set of points and the mean point of the set, as shown in Figure 7(a).

A last point is the computation of the normal sense associated to each triangle after advection by respect to grad(C)/norm (grad(C)).

3.2.3. Computation of C^{n+1}. After the advection step, several portions of polygons are present in each cell. The intersections of each polygon with the cell are computed. The mean plane for all the portions of polygon occurring in a cell has to be computed. This mean plane is fixed by a mean point and a mean normal vector, which are respectively the mean values of the centres and the normals of the polygons portions weighted by the area of the portion in the cell. An unique plane for the interface is then defined in each cell. The new VOF value C^{n+1} is then fixed as the volume of the cut cube defined by the intersection of this mean plane and the cube. This volume is computed with the formulae given in Appendix A. The situation remains the same that for 2D SL-VOF method when a cell looses the interface. The general classification of the cell types after advection is presented herafter in Figure 7(b). Figures 7(c) and 7(d) summarize the process for an A type cell.

4. BOUNDARY CONDITIONS FOR FREE SURFACES AND INTERFACES

A moving fluid boundary can be considered in two ways:

(i) If the effect of the less dense fluid (for instance air or gas) is neglected, it is not necessary to compute the flow in this fluid and the interface becomes a free surface. So the pressure at the interface (in the partial cells with $0<C<1$) is the constant gas pressure and the velocity is deduced by extrapolation of the velocity in the neighbouring cells, taking into account the weight of each cell (C value):

$$\vec{U}_{i,j,k}=\frac{\sum\sum\sum_{(l1=i-1,i+1),(l2=j-1,j+1),(l3=k-1,k+1)} C_{l1,l2,l3}\vec{U}_{l1,l2,l3}}{\sum\sum\sum_{(l1=i-1,i+1),(l2=j-1,j+1),(l3=k-1,k+1)} C_{l1,l2,l3}}$$

where $\vec{U}_{l1,l2,l3}$ is the velocity in the neighbouring cell $(l1,l2,l3)$ and $\vec{U}_{i,j,k}$ is the velocity in the cell interface (i,j,k).

(ii) If the coupling between air (or gas) and liquid is taken into account, the boundary is an interface. In this case, the Navier–Stokes equations are solved in the two fluid but also in the partial cells of interface taking account of physical local behaviour. This allows to compute more precisely the physical fields than with the single phase solver. This 2 fluid flow model does not need any particular boundary conditions on the cell's interface because the physical fields are also computed in the cells containing an interface.

5. VALIDATION OF SL-VOF 3D

5.1. Kinematics validation: advection of the sphere

5.1.1. Advecting a sphere in an uniform velocity field. A first basic test is carried out in order to verify the SL-VOF model. We consider the advection of a sphere in an uniform, constant,

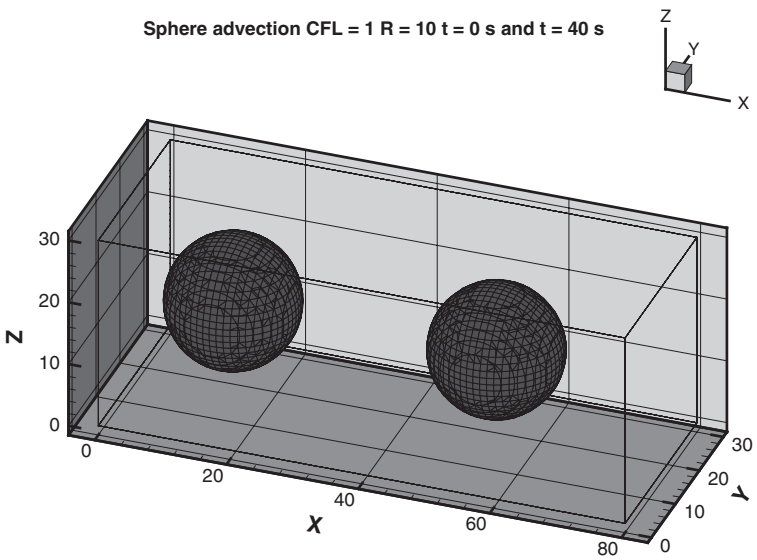

Figure 8. Advection of a sphere ($t = 0$s and 40s). The identity of the sphere is extremely well maintained.

horizontal velocity field of one cell per time step. This test case is interesting because the interface position will get all possible different orientations.

The grid contains $80 \times 30 \times 35$ cells of constant size in the three directions. The radius of the sphere is 10 cells long. Figure 8 shows the initial C field which draws the position of the interface ($0 < C < 1$) and the C field at $t = 40$ s (time step $= 40$) after advection by SL-VOF. Plate 1(a) shows the interface shape in the symmetric plane of the advection. We can observe the satisfying conservation of the interface shape during the advection even for a coarse mesh.

The tests for different velocities (CFL) and different directions of the flow give similar results. The volume of the fluid is conserved with less than $10^{-3}\%$ of error.

5.1.2. Estimation of the method's order. In order to estimate the order approximation of the method, we consider the advection of a sphere in a diagonal direction (i.e. the direction $(1, 0, 1)$ for example) for different radii of the sphere. The error estimation can be tested in two ways, either the mesh is progressively refined and the radius of the sphere remains the same, or the mesh is fixed and the radius of the sphere is progressively increased. The second solution is chosen for simplicity. We will consider the mean error, defined as $E^1 = \sum_k \mathrm{Err}_k / R \cdot n_{\mathrm{corner}}$ with Err_k the distance between the k polygon corner and the real interface, n_{corner} the total number of corners and R the radius of the sphere. The order α of the method is the value $\alpha \in R$ so that: $E^1 = \beta(h)^\alpha$, $\beta \in R$ with h the cell size. Here, it is equivalent to look for $\alpha \in R$ so that $\ln E^1 = \ln \beta - \alpha \ln(R)$. Plate 1(b) presents the mean error as a function of the radius (for seven different radius from 2 to 30) in a log/log diagram. A linear regression gives the mean slope, that is to say the order of the method. A slope of -1.65 is found. If the advection phase is supposed to be exact, the algorithm accuracy is estimated of order 1.65.

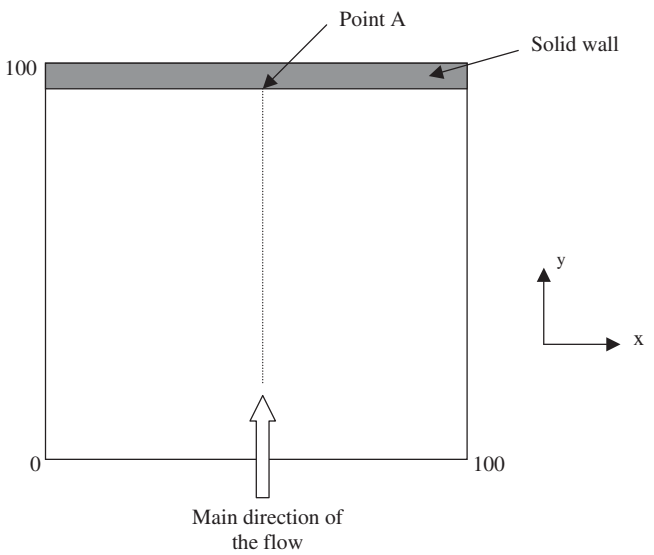

Figure 9. Scheme of the 2D computational domain for the distorting velocity field.

5.1.3. Sphere advection in a distorting velocity field. We propose here to check the ability of SL-VOF to reproduce distorted interfaces. Let us first consider the 2D potential flow generated by a solid wall perpendicular to the main direction of the flow far from the wall (see Figure 9). If $A(x_a, y_a)$ is the stagnation point where the velocity is equal to zero on the wall, one can show that the stream function of such a flow is $\Psi(x, y) = 2a(x - x_a)(y - y_a)$ with a a constant (we will take $a = 10$ for this application). Then:

$$\frac{\mathrm{d}x(t)}{\mathrm{d}t} = u(x) = 2a(x - x_a)$$

$$\frac{\mathrm{d}y(t)}{\mathrm{d}t} = v(y) = 2a(y_a - y)$$

If we consider the particles of fluid which belong to the circle of centre (x_a, y_{c0}) and of radius $R0$ for $t = 0$, one can prove that the co-ordinates $x(t)$, $y(t)$ of the particles at time t verify: $\frac{(x(t)-x_a)}{\mathrm{e}^{4at}} + \frac{(y(t)-y_c(t))}{\mathrm{e}^{-4at}} = R_0^2$ with $y_c(t)$ the ordinate of the particle located at the centre of the circle for $t = 0$. Then, in such a flow, circles are distorted progressively into ellipses of centres x_a, $y_c(t)$ and of axis $R0\mathrm{e}^{2at}$ and $R0\mathrm{e}^{-2at}$. We will consider a (100×100) computational domain. If we propagate this domain and the flow in the direction perpendicular to the plane (Oxy), we obtain a 3D computational domain with the same velocity field in each plane parallel to (Oxy). The advection of a sphere in such a flow provides ellipsoids of revolution whose analytical solution is known. We will compare then this analytical solution with the numerical solutions provided by both the standard VOF algorithm of Hirt and Nichols and our SL-VOF algorithm. The computational domain is (100,30,100) (i.e. the 2D flow in the plane Oxz is propagated over the y direction). The radius of the initial sphere is 13, and its centre is (50,15,20). In Plate 2, the velocity field in one y-slice is presented. In Figures 10(a) and

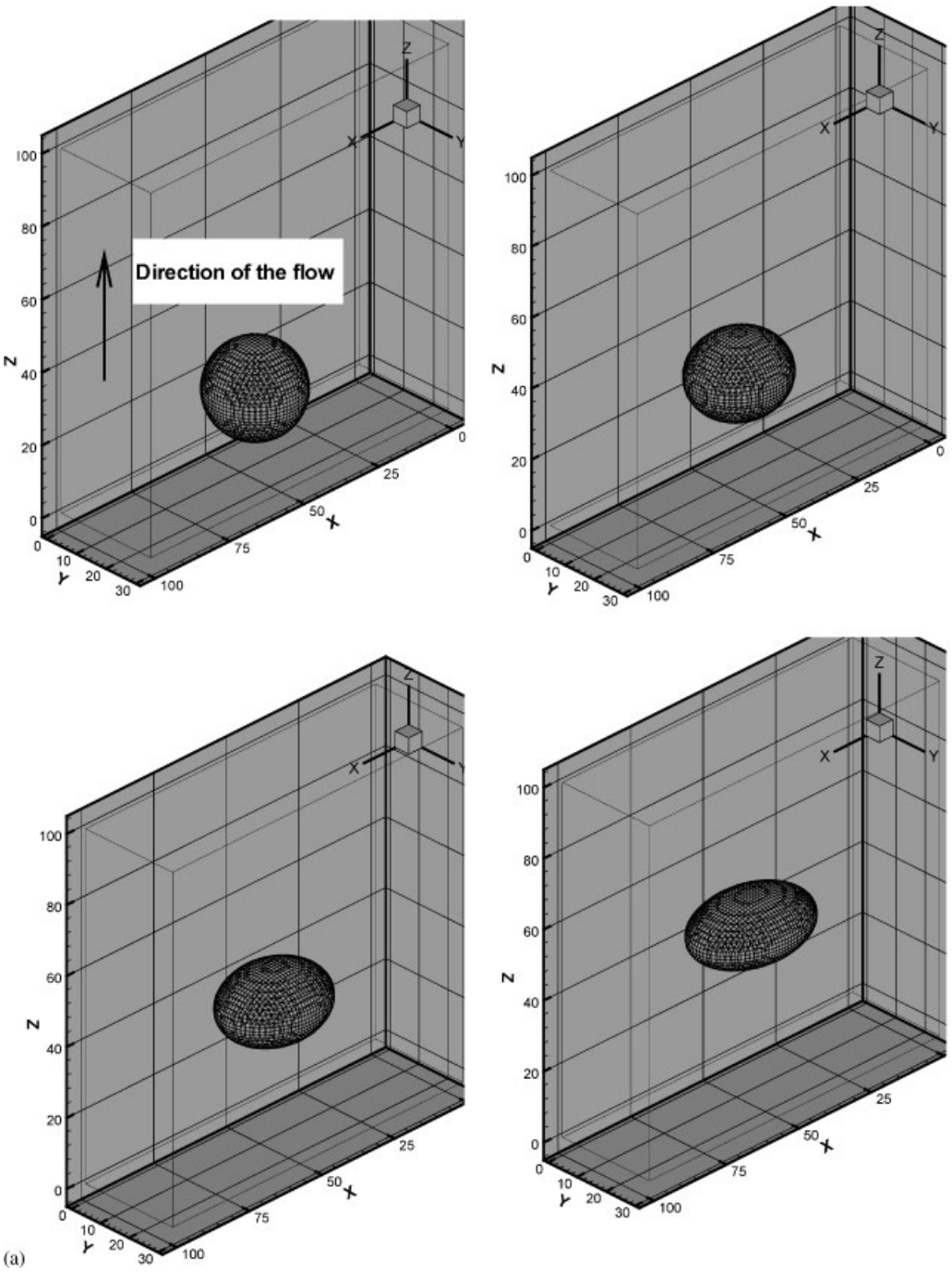

Figure 10. (a) Advection of a sphere in a distorting velocity field: impinging jet on the top wall; and (b) advection of a sphere in a distorting velocity field.

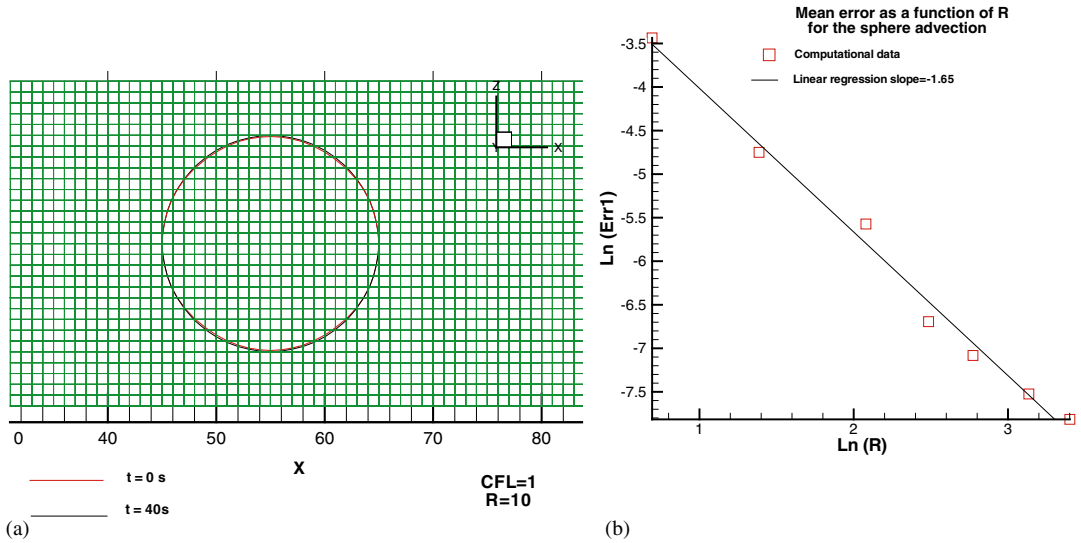

Plate 1. (a) Advection of a sphere, slice in plane *xz* (red lines = translated initial VOF contour/black lines = VOF contour after 40 time iterations/green lines = grid); and (b) order of the method (mean error as a function of R).

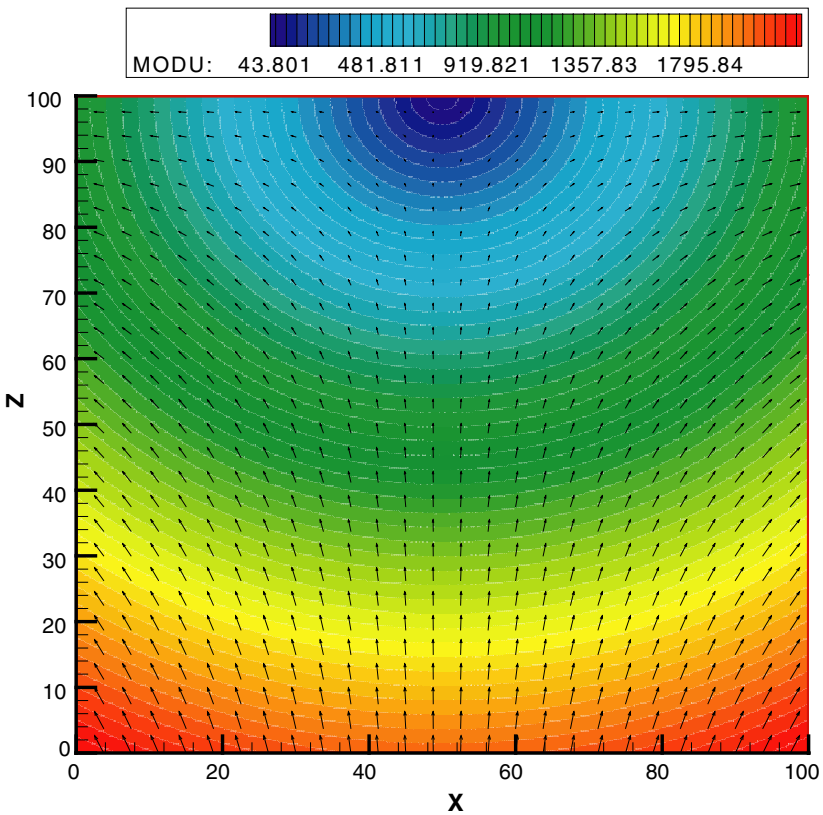

Plate 2. Velocity field in a *y*-slice.

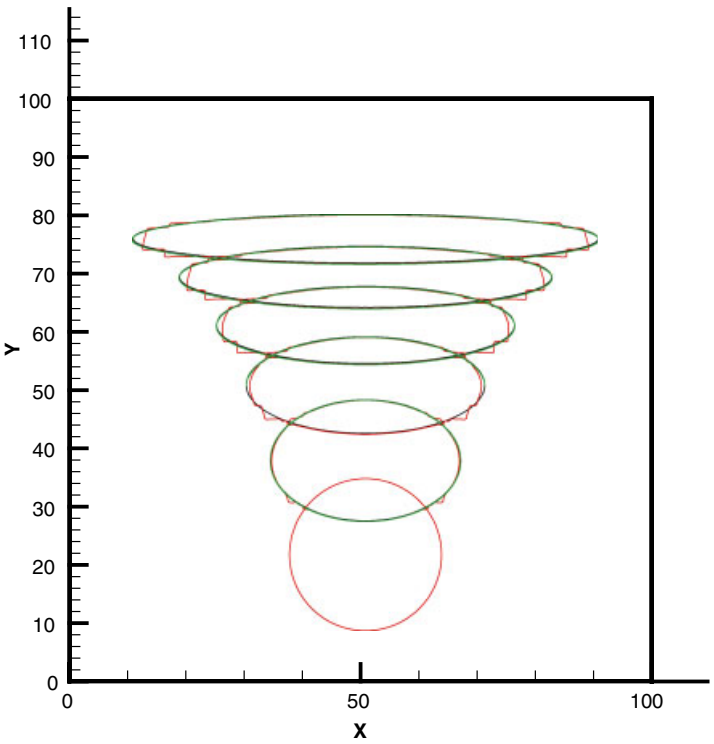

Plate 3. Comparisons for different time steps between the analytical solution, the SL-VOF solution and the Hirt and Nichols algorithm solution.

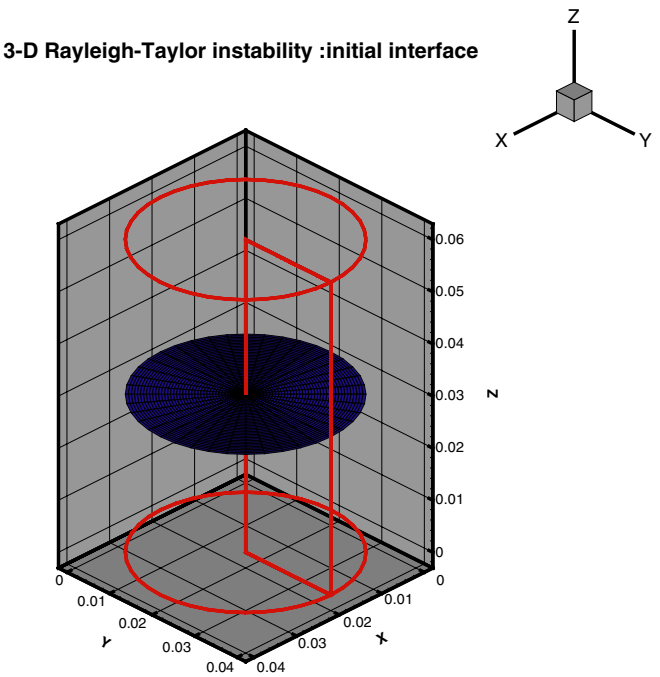

Plate 4. 3D Rayleigh–Taylor instability (initial interface is the blue surface).

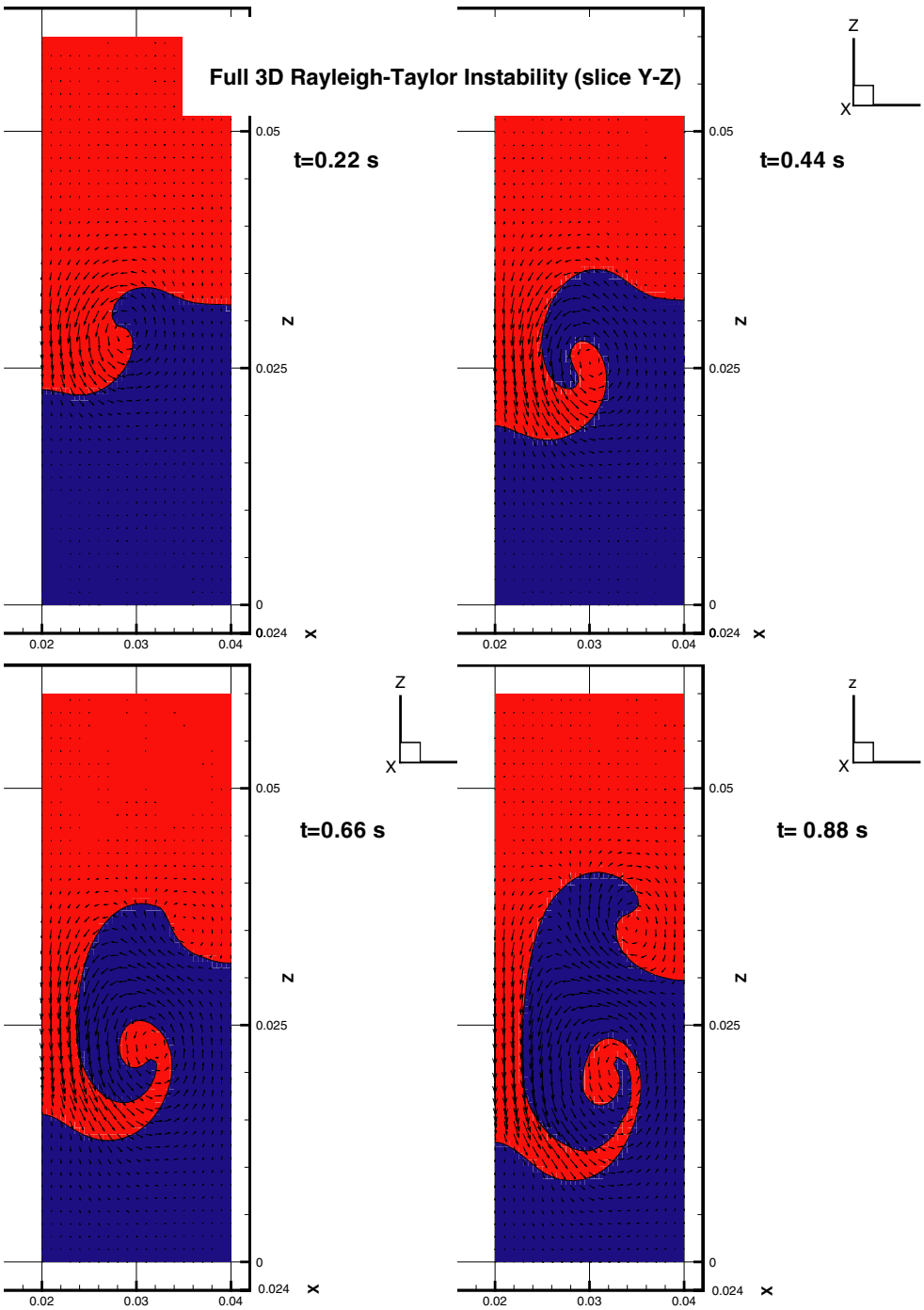

Plate 5. 3D Rayleigh–Taylor instability (views on the meridian plane X–Z). The velocity vectors are represented for every two grid cells.

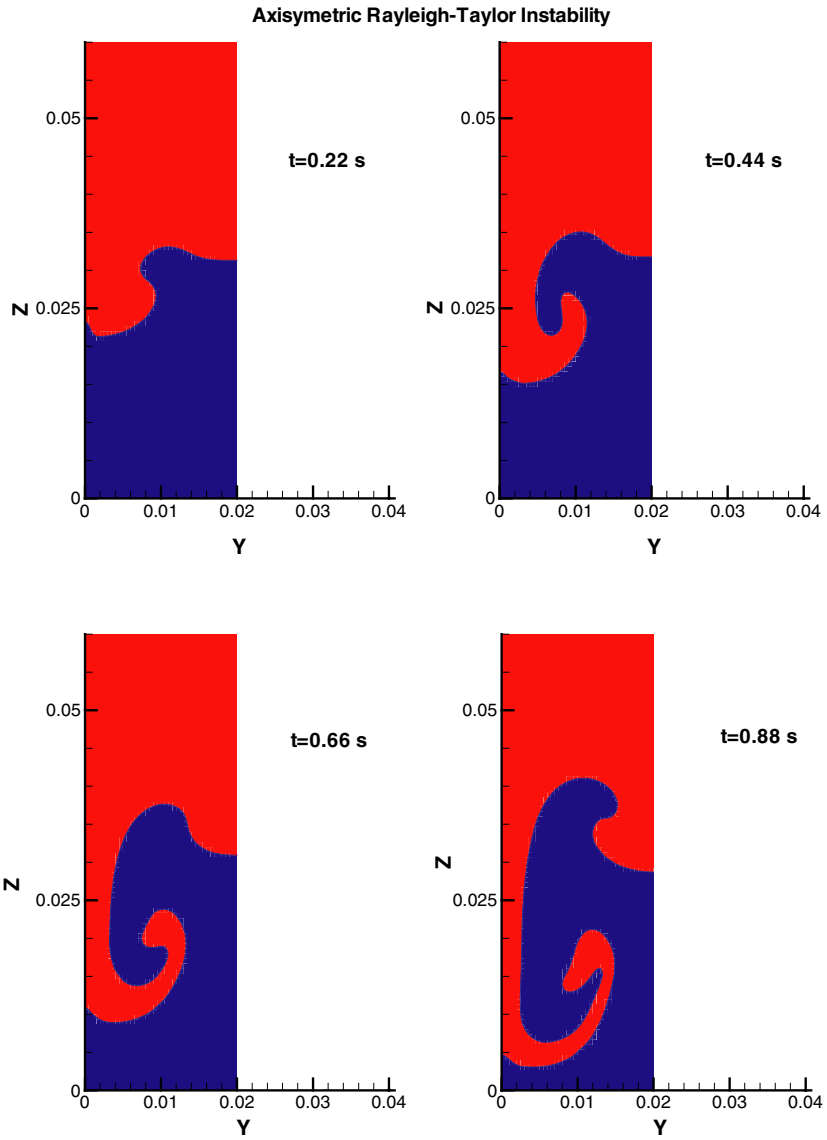

Plate 6. Axisymmetric Rayleigh–Taylor instability with SL-VOF 2D.

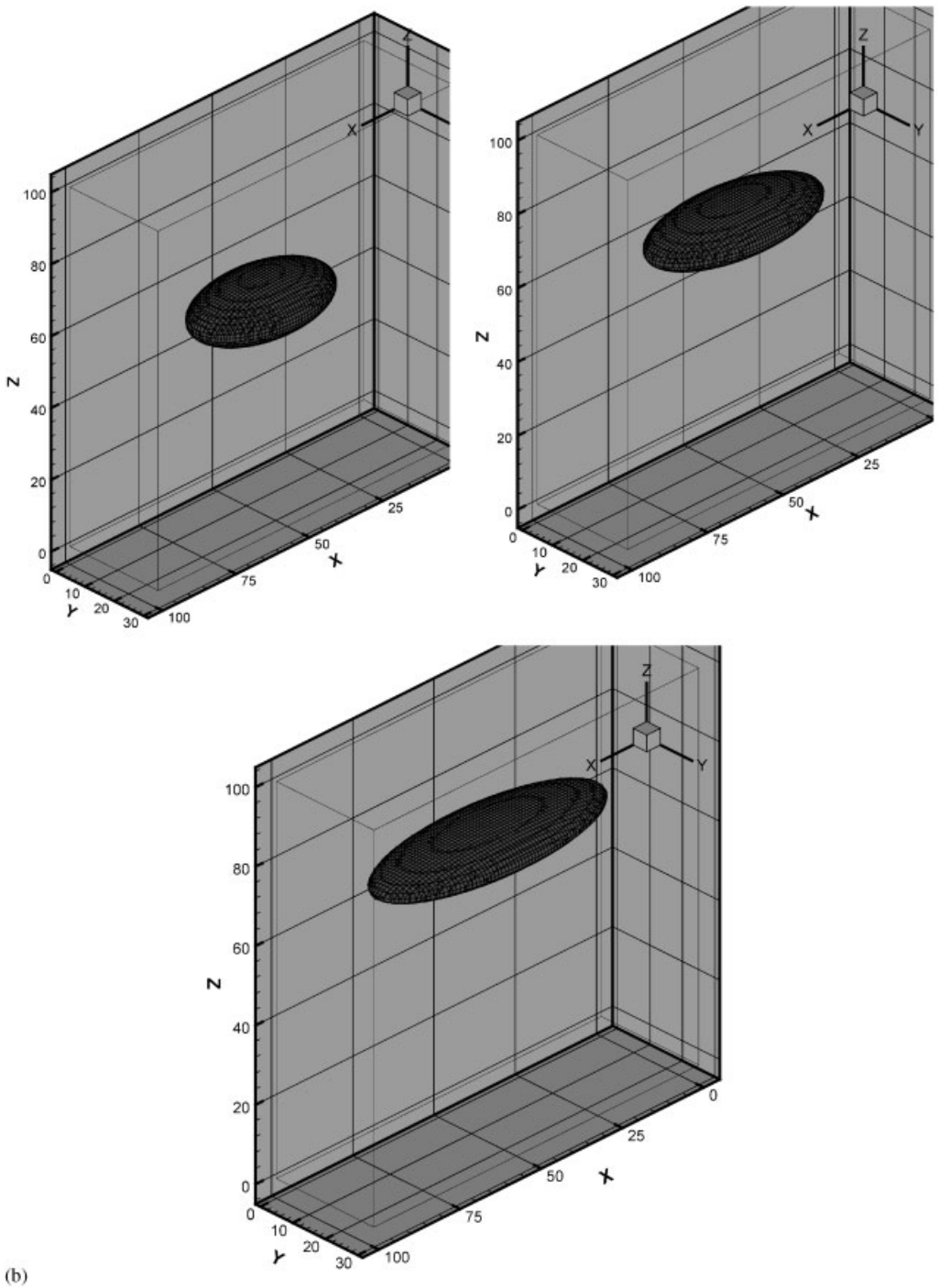

(b)

Figure 10. *Continued.*

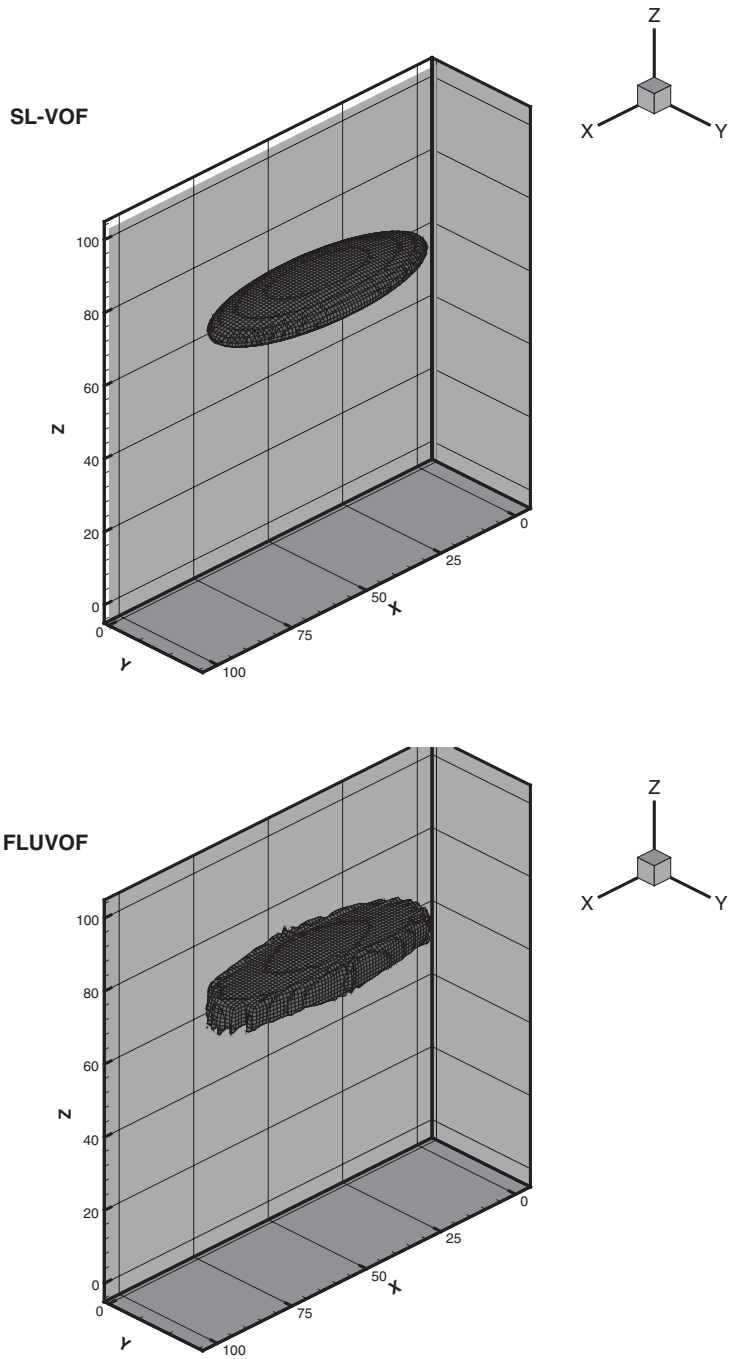

Figure 11. Comparisons between SL-VOF and original VOF numerical solutions.

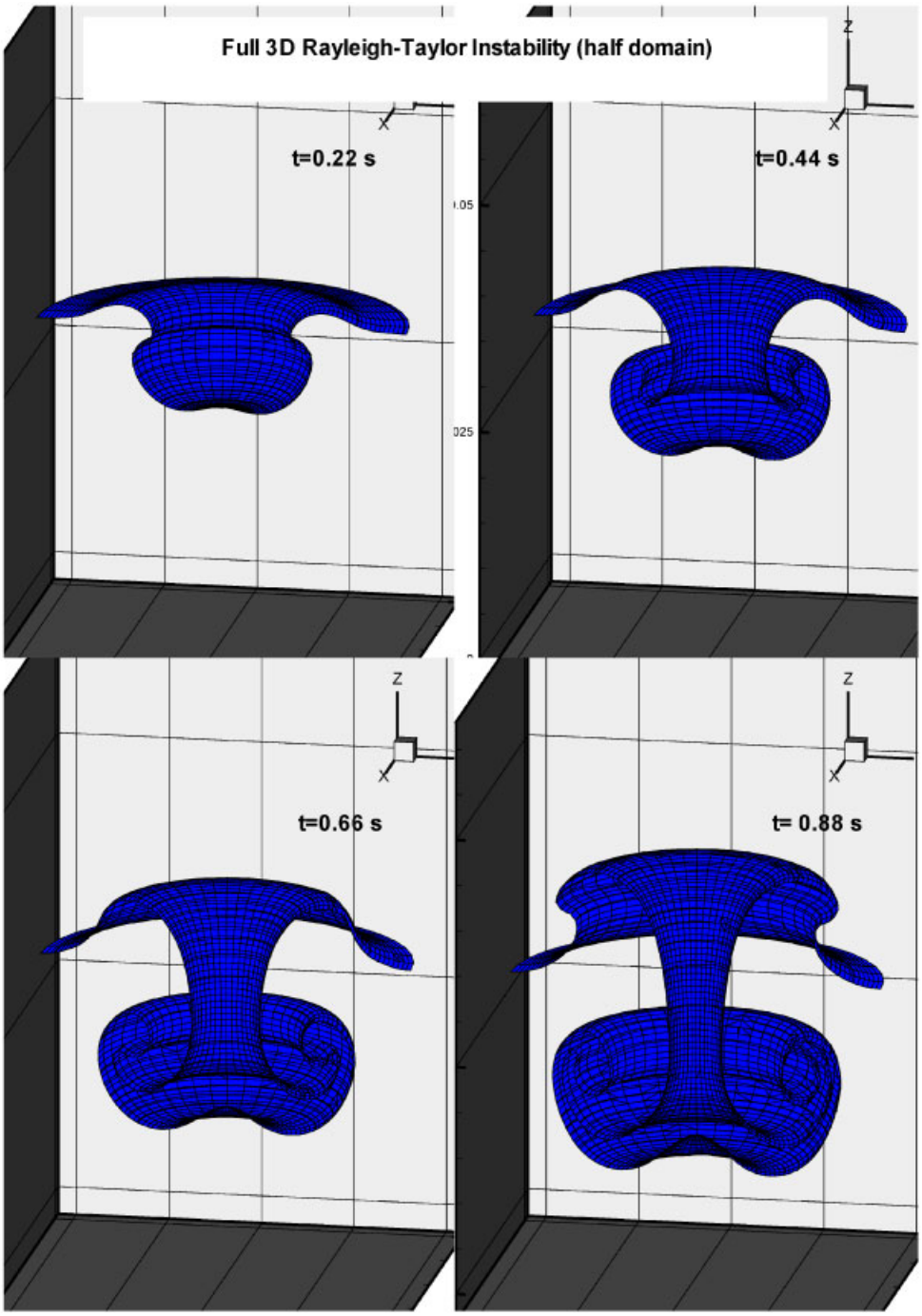

Figure 12. 3D Rayleigh–Taylor instability (evolution of the interface).

10(b) the VOF contours computed using SL-VOF for different time steps of the simulation are shown.

It is easy to compare the analytical and the numerical solutions in the mid-plane $y = 15$. In Plate 3 the analytical solution, the numerical solution computed by SL-VOF and the numerical solution computed by the original VOF algorithm of Hirt and Nichols are shown.

The solution computed by SL-VOF is very close to the analytical solution, by contrary to the Hirt and Nichols algorithm solution which is not able to accurately describe the ellipsoid's extremities. This is one of the advantages of the PLIC model as compared to the SLIC one: when the curvature of the interface is increasing, the SLIC model requires a high number of cells to describe the interface. Moreover, the Lagrangian advection allows to use high CFL numbers whereas the flux advection proposed in the Hirt and Nichols algorithm forbids CFL greater that 0.5. For this simulation, SL-VOF is five times faster than the original VOF method. The maximal error observed on the position of the interface is about half a cell with SL-VOF for five cells with the original VOF method. Figure 11 shows the interface contours computed for the same time by SL-VOF and the original VOF method.

5.2. Dynamics validation: Rayleigh–Taylor instability

We now consider the Rayleigh–Taylor instability test case which is characterized by a complex flow problem with a highly non-linear interface shape evolution. A number of authors have been interested by this flow (see References [6, 11–13] for example).

We consider two inviscid fluids of different densities superposed in a cylindrical tank of 6 cm height and 2 cm radius. The fluid densities are 1 for the lower fluid and 2 for the upper fluid. The Navier–Stokes equations are solved in the two fluids. The surface tension is neglected.

The cylindrical mesh is of $40 * 40 * 90$ cells.

An initial plane interface is imposed in the middle height of the cylindrical tank (Plate 4). The initial perturbation of the interface is imposed by a sinusoidal velocity perturbation characterized by a maximal velocity ($W = -1$ m/s) on the symmetrical axis of the tank, a minimal velocity near the wall ($W = 0$) and a wavelength $= 0.02$ m.

The interface evolution between the two fluids for four different times (0.22, 0.44, 0.66 and 0.88 s) is given in Figure 12. Only half of the domain is shown.

The geometrical symmetry of the interface is observed to be satisfied.

It is interesting to compare this 3D simulation with an axisymmetric simulation of the same Rayleigh–Taylor instability carried out with the SLVOF 2D model.

Plates 5 and 6 show, respectively, the evolution of the interface, at the same times, for the 3D simulation (on a meridian symmetrical plane, the red rectangle on Plate 4) and for the 2D simulation. The red fluid is the denser one. A very good agreement between the two simulation is observed.

6. CONCLUSION

The extension of the newly proposed 2D SL-VOF numerical method for interface tracking to 3D flows has been performed. Several test cases like advection of a sphere and fully 3D Rayleigh–Taylor instability have been successfully computed. The comparisons with both

original VOF method and SL-VOF method for 2D flows have shown that SL-VOF 3D is able to simulate complex two-phase flows with first order accuracy for significant deformations of the interface. PLIC modelling and Lagrangian advection allows to increase both accuracy and time steps. Advecting a sphere in a distorting velocity field shows that SL-VOF method is at least five times faster than the basic VOF method of Hirt and Nichols. The large computational time required for 3D simulations is then reduced. The order of the method being about 1.65, the accuracy is highly improved when great deformations of the interface occur. The accuracy and the capability to represent complex interfaces of SL-VOF 3D will allow to use the method in a near future for coastal applications, such that wave breaking and sedimentary transport, where large deformations of the interfaces occurs. The next developments of the method will lead on the coupling with a BIEM method, in order to decrease once more computational times, and on the involvement of a subscale turbulence model in order to describe precisely the small structures for high Reynolds numbers.

APPENDIX: A TRANSLATION OF THE PLANES IN THE GRID CELLS AS A FUNCTION OF THE VOF AND THE NORMALS (CALCULATION OF α)

A.1. Geometric configuration

Let us consider the cube ABCDEFGH (Figure A1) of sides $AB = AH = AD = 1$. A cartesian reference system of origin A is linked to the cube. The cube is intersected by the plane IJK. Let us note (n, m, l) the normal to the plane. The equation of the plane is then: $mx_1 + nx_2 + lx_3 = \alpha$. Moreover: $AI = \alpha/m$, $AJ = \alpha/n$ and $AK = \alpha/l$. With a view to determine the volume under the interface, i.e. the volume ABGHLMNK, one begins by finding the volume of the tetrahedron

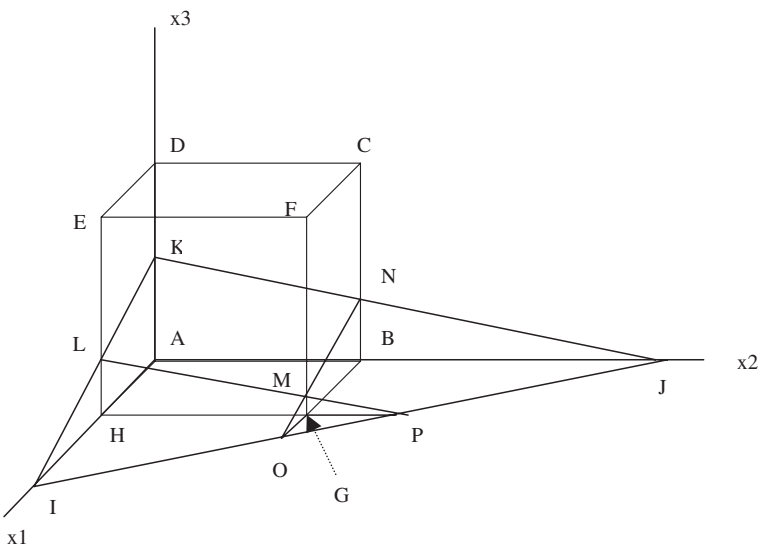

Figure A1. Cut cube by the plane describing the interface.

AIJK, which is: $\alpha^3/6mnl$. Then, it is necessary to subtract the volumes of the exterior tetrahedrons (HIPL and BOJN in Figure A1). Those tetrahedrons are geometrically similar to AIJK, and the ratios of their volume to the volume AIJK are $(1-m/\alpha)^3$ and $(1-n/\alpha)^3$, respectively. One has then to consider that the volume of GOPM is subtracted twice (if the segment IJ is not included in the rectangle ABGH), so that the volume of GOPM has to be added to the final result. One can show that the ratio of the volume GOPM to the volume AIJK is $(1-m/\alpha-n/\alpha)^3$. Moreover, if the point K is located above the point D on the axis $(O,x3)$, the volume of the tetrahedron intercepting K and D above the cube has to be subtracted too: the ratio of this tetrahedron's volume to the volume AIJK is then $(1-l/\alpha)^3$. It is now possible to determine the volume of the cut cube.

Several cases has to be examined. One can remark that when α increases from 0 to $n+m+l$, the volume increases from 0 to 1. The expression of the volume depends then on the geometrical shape of the cut cube. When α increases from 0 to $m+n+l$, the plane intercepts six corners successively. This corresponds to six different shapes of the cut cube and then to six different expressions for the volume.

A.2. Calculation of the critical volumic fractions

The order in which the plane intercepts the corner $(1,1,0)$ and the corner $(0,0,1)$ depends on the comparison between $m+n$ and l. Two cases have to be examined:

- case $m+n<l$, i.e. the corner $(1,1,0)$ is intercepted before the corner $(0,0,1)$,
- case $m+n>l$, i.e. the corner $(0,0,1)$ is intercepted before the corner $(1,1,0)$.

A.2.1. Case: $m+n<l$. Hereafter are the six configurations corresponding to the six critical volumes.

Let us determine the six critical volumes of those configurations.

(1°) *Volumic fraction* $C1$ (*case* (*a*) *in Figure* A2): In this case, the plane intercepts the point $(1,0,0)$, so that $\alpha=m$. The volumic fraction of the cut cube is here the volume of AIJK because the points I and J are inside the cube. Thus, $C1=\alpha^3/6mnl$ and:

$$C1=\frac{m^2}{6nl}$$

(2°) *Volumic fraction* $C2$ (*case* (*b*) *in Figure A2*): In this case, the plane intercepts the point $(0,1,0)$, so that $\alpha=n$. The volumic fraction of the cut cube is here the volume of AIJK to which is subtracted the volume of HIPL. Thus, $C2=(\alpha^3/6mnl)[1-(1-m/\alpha)^3]$. And:

$$C2=\frac{3n-3nm+m}{6nl}$$

(3°) *Volumic fraction* $C3$ (*case* (*c*) *in Figure A2*): In this case, the plane intercepts the point $(1,1,0)$ so that $\alpha=m+n$. The volumic fraction of the cut cube is here the volume of AIJK to which is subtracted the volumes HIPL and BOJN.

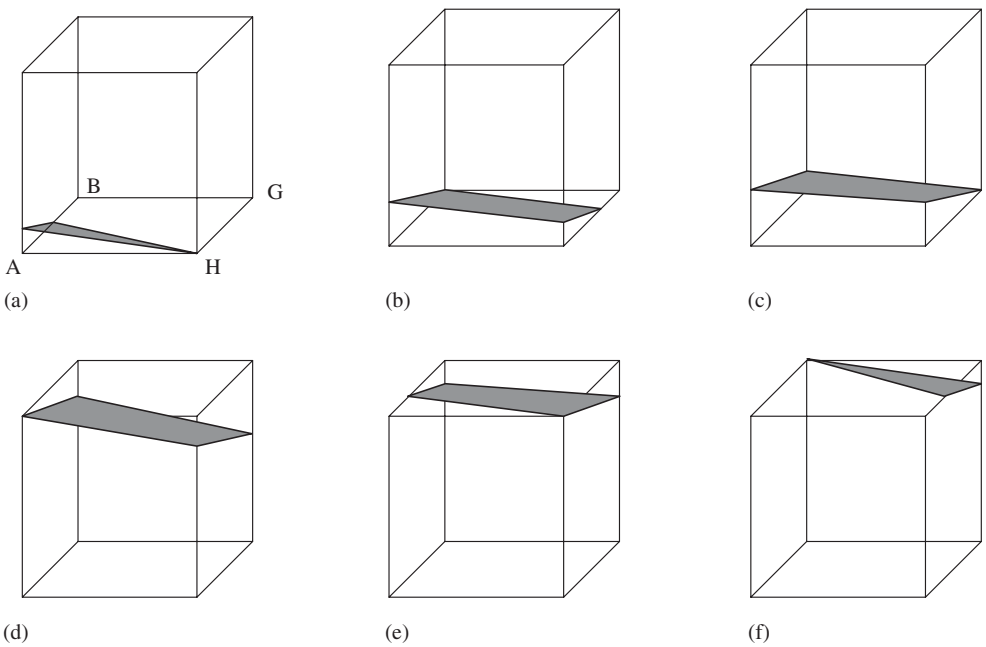

Figure A2. Critical volumes in the case $m+n<l$.

Thus, $C3=(\alpha^3/6mnl)[1-(1-m/\alpha)^3-(1-n/\alpha)^3]$. And:

$$C3=(m+n)/2l$$

(4°) *Volumic fractions* $C4$, $C5$ *and* $C6$ (*cases* (*d*), (*e*), (*f*) *in Figure A2*): The volumic fractions C4, C5 and C6 are deduced from $C1$, $C2$, $C3$ by symmetry. Thus:

$$C4=1-C3$$

$$C5=1-C2$$

$$C6=1-C1$$

A.2.2. case: $m+n>l$. Hereafter are the six volumic fractions corresponding to this case.

In this case, the critical volumic fractions corresponding to (g) and (h) in Figure A3 are calculated in the same way that for the case $m+n<l$. Thus:

$$C1=\frac{m^2}{6nl}$$

$$C2=\frac{3n^2-3nm+m^2}{6nl}$$

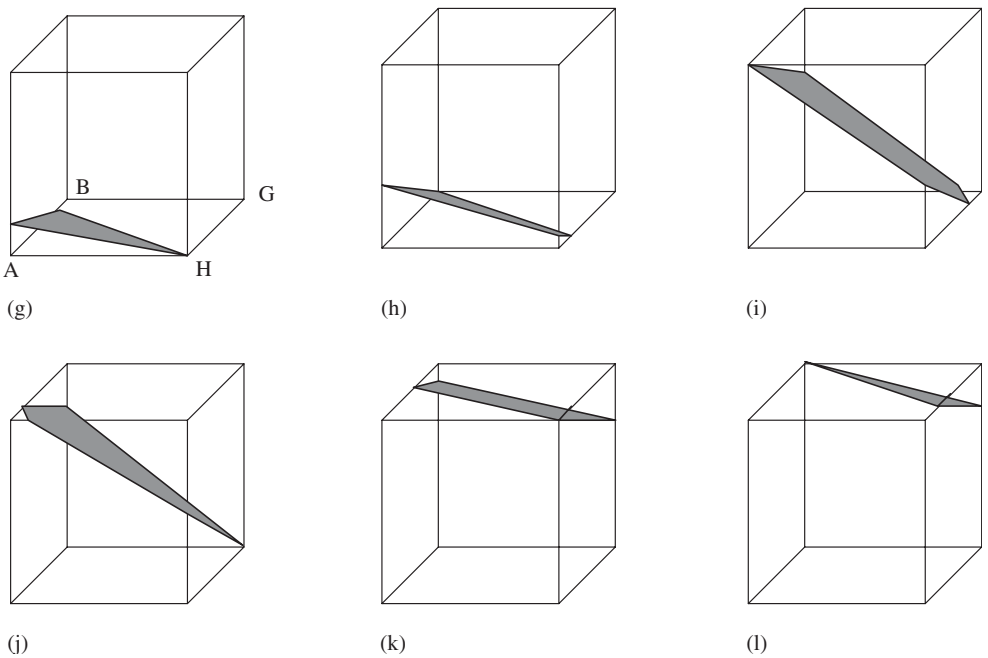

Figure A3. Critical volumes in the case $m+n>l$.

For the case in (i) in Figure A3, the plane intercepts the point $(0,0,1)$, so that $\alpha = l$. The volumic fraction is the volume AIJK to which is subtracted the volumes HIPL and BOJN.

Thus:

$$C3 = \frac{\alpha^3}{6mnl}\left[1 - \left(1 - \frac{m}{\alpha}\right)^3 - \left(1 - \frac{n}{\alpha}\right)^3\right]$$

$$= \frac{1}{6mnl}\left[l^3 - (l-m)^3 - (l-n)^3\right]$$

And:

$$C3 = \frac{1}{6mnl}\left[l^3 - (l-m)^3 - (l-n)^3\right]$$

$C4$, $C5$ and $C6$ are deduced by symmetry:

$$C4 = 1 - C3$$

$$C5 = 1 - C2$$

$$C6 = 1 - C1$$

A.3. Calculation of α and shape of the intersection polygon

A.3.1. Case $m+n<l$

- If $0<C<C1$ (i.e. $0<\alpha<m$), the intersection polygon is here a triangle of corners $(\alpha/m,0,0)$, $(0,\alpha/n,0)$ and $(0,0,\alpha/l)$. Moreover, the volume is in this case $C=\alpha^3/6mnl$. Thus:

$$\alpha=\sqrt[3]{6Cmnl}$$

- If $C1\leqslant C<C2$ (i.e. $m\leqslant\alpha<n$), the intersection polygon is here a quadrilateral of corners $(0,0,\alpha/l)$, $(1,0,(\alpha-m)/l)$, $(1,(\alpha-n)/l,0)$ and $(0,\alpha/n,0)$. Moreover, the volume is in this case:
  $C=\frac{1}{6mnl}[\alpha^3-(\alpha-m)^3]$. Thus:

$$\alpha^2-m\alpha+\frac{m^2}{3}-2nlC=0$$

  Only the root $m+\sqrt{8nlC-(m^2/3)}$ corresponds to the criterion $m<\alpha$, thus:

$$\alpha=m+\sqrt{8nlC-\frac{m^2}{3}}$$

- If $C2\leqslant C<C3$ (i.e. $n\leqslant\alpha<m+n$), the intersection polygon is a pentagon of corners $(1,0,(\alpha-m)/l)$, $(1,(\alpha-m)/n,0)$, $((\alpha-n)/m,1,0)$, $(0,1,(\alpha-n)/l)$ and $(0,0,\alpha/l)$. The volume is in this case: $C=(1/6mnl)[\alpha^3-(\alpha-m)^3-(\alpha-n)^3]$. Thus:

$$-\alpha^3+3(m+n)\alpha^2-3(m^2+n^2)\alpha+m^3+n^3-6mnlC=0$$

  This equation is solved numerically by a bisection method. The right root is the one corresponding to the criterion $n\leqslant\alpha<m+n$.
- If $C3\leqslant C<C4$ (i.e. $m+n\leqslant\alpha<l$), the intersection polygon is a quadrilateral of corners $(1,0,\alpha-m/l)$, $(1,1,\alpha-m-n/l)$, $(0,1,\alpha-n/l)$ and $(0,0,\alpha/l)$. The volume is: $C=(1/6mnl)[\alpha^3-(\alpha-m)^3-(\alpha-n)^3+(\alpha-m-n)^3]$, expression which reduces to: $C=(1/l)(\alpha-(m+n)/2)$, so that:

$$\alpha=\frac{1}{2}(2Cl+m+n)$$

  All the others cases are found by symmetry.

A.3.2. Case $m+n>l$. For the first three cases, the formulae are the same that previously. It is to say:

- If $0<C<C1$ (i.e. $0<\alpha<m$), the intersection polygon is a triangle de sommets $(\alpha/m,0,0)$, $(0,\alpha/n,0)$ and $(0,0,\alpha/l)$, so:

$$\alpha=\sqrt[3]{6Cmnl}$$

- If $C1 \leqslant C < C2$ (i.e. $m \leqslant \alpha < n$), the intersection polygon is a quadrilateral of corners $(0,0,\alpha/l)$, $(1,0,(\alpha-m)/l)$, $(1,(\alpha-n)/l,0)$ and $(0,\alpha/n,0)$, so:

$$\alpha = m + \sqrt{8nlC - \frac{m^2}{3}}$$

- If $C2 \leqslant C < C3$ (i.e. $n \leqslant \alpha < l$), the intersection polygon is a pentagon of corners $(1,0,(\alpha-m)/l)$, $(1,(\alpha-m)/n,0)$, $((\alpha-n)/m,1,0)$, $(0,1,(\alpha-n)/l)$ and $(0,0,\alpha/l)$. α is calculated by solving the equation:

$$-\alpha^3 + 3(m+n)\alpha^2 - 3(m^2+n^2)\alpha + m^3 + n^3 - 6mnlC = 0$$

On the other hand, if $C3 \leqslant C < C4$ (i.e $l \leqslant \alpha < m+n$), the formula is different. In this case, the intersection polygon is a hexagon of corners $(1,0,(\alpha-m)/l)$, $(1,(\alpha-m)/n,0)$, $((\alpha-n)/m,1,0)$, $(0,1,(\alpha-n)/l)$, $(0,(\alpha-l)/n,1)$ and $((\alpha-l)/m,0,1)$. The volume is here $C = \frac{1}{6mnl}[\alpha^3 - (\alpha-m)^3 - (\alpha-n)^3 - (\alpha-l)^3]$. Then:

$$-2\alpha^3 + 3(m+n+l)\alpha^2 - 3(m^2+n^2+l^2)\alpha + m^3 + n^3 + l^3 - 6mnlC = 0$$

This equation is solved, and the right root is the one satisfying $l \leqslant \alpha < m+n$.

ACKNOWLEDGEMENTS

Financial support to Benjamin Biausser by Principia R. and D. and by the french national Programme Océan-Atmosphère Multi-echelles P.A.T.O.M are gratefully acknowledged.

Ib Svendsen is acknowledged for helpful consultation of the paper.

REFERENCES

1. Hyman JM. Numerical method for tracking interfaces. *Physica D* 1984; **12**:396–407.
2. Laget O. Résolution des équations d'Euler pour des écoulements non-linéaires en présence d"ne interface. *Thèse de Doctorat*, Université de Nice, 1998.
3. Grilli ST, Svendsen IA, Subramanya R. Breaking criterion and characteristics for solitary wave breaking on slopes. *Journal of Waterway Port C, ASCE* 1997; **123**(3):102–112.
4. Hirt CW, Nichols BD. Volume of fluid method for the dynamics of free boundaries. *Journal of Computational Physics* 1981; **39**:323–345.
5. Li J. Piecewise linear interface calculation. *Comptes Rendus de l Academie des Sciences Serie II. Fascicule B—Mecanique* 1995; **320**:391–396.
6. Guignard S, Marcer R, Rey V, Kharif C, Fraunié P. Solitary wave breaking on sloping beaches: 2D two phase flow numerical simulation by SL-VOF method. *European Journal of Mechanics B—Fluids* 2001; **20**:57–74.
7. Viviand H. Analysis of pseudo-compressibility systems for compressible and incompressible flows. In *Computational Fluid Dynamics*, Review 1995. Oshima H (ed.), Wiley: New York, 1995.
8. De Jouëtte C, Viviand H, Wornom S, Le Gouez JM. Pseudo compressibility method for incompressible flow calculation. *4th International Symposium on Computational Fluid Dynamics*, California, Davis, 9–12 September, 1991.
9. Jameson A, Schmidt A, Turkel E. Numerical solutions for the Euler equations by finite volumes methods using Runge–Kutta time-marching schemes. *AIAA 14th Fluid and Plasma Dynamics*, *Conference*, Palo Alto, California, June 1981.
10. Abadie S. Modélisation du déferlement plongeant par une méthode VOF. *Thèse de Doctorat*, Université de Bordeaux I, 1998.
11. Lord Rayleigh. *Scientific Papers*, vol ii. Cambridge University Press, Cambridge, UK, 1900; p. 200.
12. Tryggvason G. Numerical Simulations of the Rayleigh–Taylor Instability. *Journal of Computational Physics* 1988; **75**:253–282.
13. Chandrasekhar S. The character of the equilibrium of an incompressible heavy viscous fluid of variable density. *Proceedings of the Cambridge Philosophical Society* 1955; **51**:162.

